IRAQI Academic Scientific Journals
Samarra Journal of Pure and Applied Science
SJPAS
مجلة سامراء للعلوم البحتة والتطبيقية
www.sjpas.com
p ISSN: 2663-7405
e ISSN: 2789-6838

Assessment of Boron-Modified Semicarbazide and Thiosemicarbazide Resins as Corrosion Inhibitors for Carbon Steel Alloy in Acidic Environment

Mustafa F. A.*, Saki T. A., Hadi Z. M.
Department of Chemistry, Science Collage, University of Basra, Iraq.

https://doi.org/10.54153/sjpas.2025.v7i1.854

Article Information
Received: 23/03/2024
Revised: 20/04/2024
Accepted: 10/06/2024
Published: 30/03/2025

Keywords:
Semicarbazide-Formaldehyde, Thiosemicarbazide-Formaldehyde, Boric acid, Corrosion Inhibitors, and Resins.

Corresponding Author

E-mail: Tahseen.saki@uobasrah.edu.iq
Mobile: +964 781 192 3127

Abstract

This study aims to synthesize two types of resins derived from semicarbazide and thiosemicarbazide for use as corrosion inhibitors. boron-Modified semicarbazide-formaldehyde resin (SFB) derived from semicarbazide, formaldehyde, and boric acid, and the other inhibitor boron-Modified thiosemicarbazide-formaldehyde resin (TSFB) derived from thiosemicarbazide, formaldehyde, and boric acid, they were studied using FTIR and TGA techniques. They were evaluated as inhibitors of corrosion of carbon steel alloy in a corrosive acidic environment of 0.1 M hydrochloric acid at several temperatures (25, 35, 45, 55) °C and at different concentrations for both inhibitors separately, using the Tafel extrapolation method. Where (SFB) gave the best inhibition efficiency at a concentration of 4 ppm, whereas the best inhibition efficiency was For (TSFB) at a concentration of 10 ppm. The investigation focused on activation parameters like E_a, ΔH^* and ΔS^*. It was observed that the activation energy was higher when an inhibitor was present than when it was absent. Additionally, the research revealed that the corrosion reaction is exothermic. The activation entropy demonstrated an increase in the number of corrosive species at elevated temperatures, which is attributed to the increased kinetic energy of these species as they interact with the alloy surface.

Introduction

Carbon steels are widely used in industrial pipelines and as structural alloys [1]. Corrosion is the process by which metals and alloys react with their surroundings and undergo chemical or electrochemical changes. The anode, cathode, electrical circuit, and electrolyte solution are all parts of a cell system that are susceptible to corrosion, which can lead to the destruction and reduction in the lifespan of metal equipment [2,3]. Several methods can be used to prevent or reduce the corrosion of metals and alloys. One such method is the use of corrosion inhibitors, which are substances that, when added in appropriate concentrations, reduce or prevent corrosion [4]. According to the literature, inhibitors containing S are beneficial in solutions containing sulfuric acid, whereas inhibitors containing N function better in solutions containing hydrochloric acid [5]. The most regulated method for safeguarding property against deteriorating corrosion is still a polyurea coating.

This makes it the most effective corrosion protection method available. However, large-scale industrial metals are typically the focus of corrosion protection offered by a polyurea coating. However, one should consider applying a polyurea coating, even for private use, such as in copper fences [6]. Polymeric chains rich in long-chain amines are frequently used as protective coatings against corrosion, particularly those derived from elongated fatty acid molecules, which confer extended durability due to the protective layer [7]. The critical role of chain length and specific substituents in amines in attaining the requisite anticorrosive traits has been reaffirmed by research [8]. Multiple patents have detailed various polyamine molecular modifications designed to enhance their effectiveness as corrosion preventatives [9]. Thiourea and its derivatives have long been studied as interesting organic inhibitors of corrosion, especially for iron and steel. In addition, thiourea, along with its various forms, have been thoroughly examined as promising organic protestants against corrosion, particularly for metals such as iron and steel [10]. The creation of new types of nontoxic corrosion inhibitors that are free from heavy metals and organic phosphates is highly significant [10]. Although widely applied across multiple contexts for diverse metals and alloys, the use of inorganic substances like chromates, dichromates, nitrates, and nitrites is now under scrutiny due to their well-documented harmful biological effects, notably those of chromates [11], along with their environmental implications [12]. The primary function of corrosion inhibitors is to reduce the onset of flash rust on metal surfaces, thereby extending the period before repainting is necessary [13]. However, inhibitory compounds that dissolve into soluble salts pose a risk of invisible contamination on metal surfaces before the application of costs, potentially leading to early failures in paint applications [14]. One agent effective in preventing flash rust is sodium tetraborate (borax), which is water-soluble and classified as an anodic inhibitor [15]. Furthermore, polymers modified with boric acid showcase ease of production, affordability, and desirable thermal characteristics, as documented in prior studies [16].

Materials and methods

Chemicals

A 30% formalin solution was obtained from RDH Chemical Company, sodium hydroxide from Himedia, semicarbazide and thiosemicarbazide from Thomas Baker, boric acid from Spectrum Chemical, phosphoric acid from Fluka, ethanol from Alpha Chemika, and hydrochloric acid from SDFCL.

Experiments

Synthesis of Semicarbazide formaldehyde resins containing boric acid (SFB)

Semicarbazide (7.5 g) was dissolved in 10 mL of water and mixed in a 100 mL beaker with 30 mL of formaldehyde solution at pH 9-10. Sodium hydroxide at 60 °C was then added to the mixture with continuous stirring using a magnetic stir bar. After 3 h, dilute phosphoric acid was added to reduce the alkalinity and achieve a pH of 7 [17]. Subsequently, the mixture was washed several times with ethanol, resulting in the formation of a white, gum-like substance. Next, 0.4 g of an aqueous solution of boric acid was added to 4 g of the product in a 50 mL beaker while heating and stirring continuously for 30 min at 60 °C [18]. After the solvent had evaporated, a white solid was obtained (Fig. 1a).

Synthesis of Thiosemicarbazide formaldehyde resins containing boric acid (TSFB)

Thiosemicarbazide (9.1 g) was dissolved in 10 mL of DMF and mixed in a 100 mL beaker with 30 mL of formaldehyde solution at pH 9-10. Sodium hydroxide at 60 °C was then added to the mixture with continuous stirring using a Magnetic Stir Bar. After 3 h, dilute phosphoric acid was added to reduce the alkalinity and achieve pH 7. Subsequently, the mixture was washed several times with ethanol, during which a white substance similar to gum formed. Next, 0.4 g of an aqueous solution of Boric acid was added to 4 g of the product in a 50 mL beaker while heating and stirring continuously for 30 min at 60 °C. After evaporating the solvent, an orange solid was obtained (Fig. 1b).

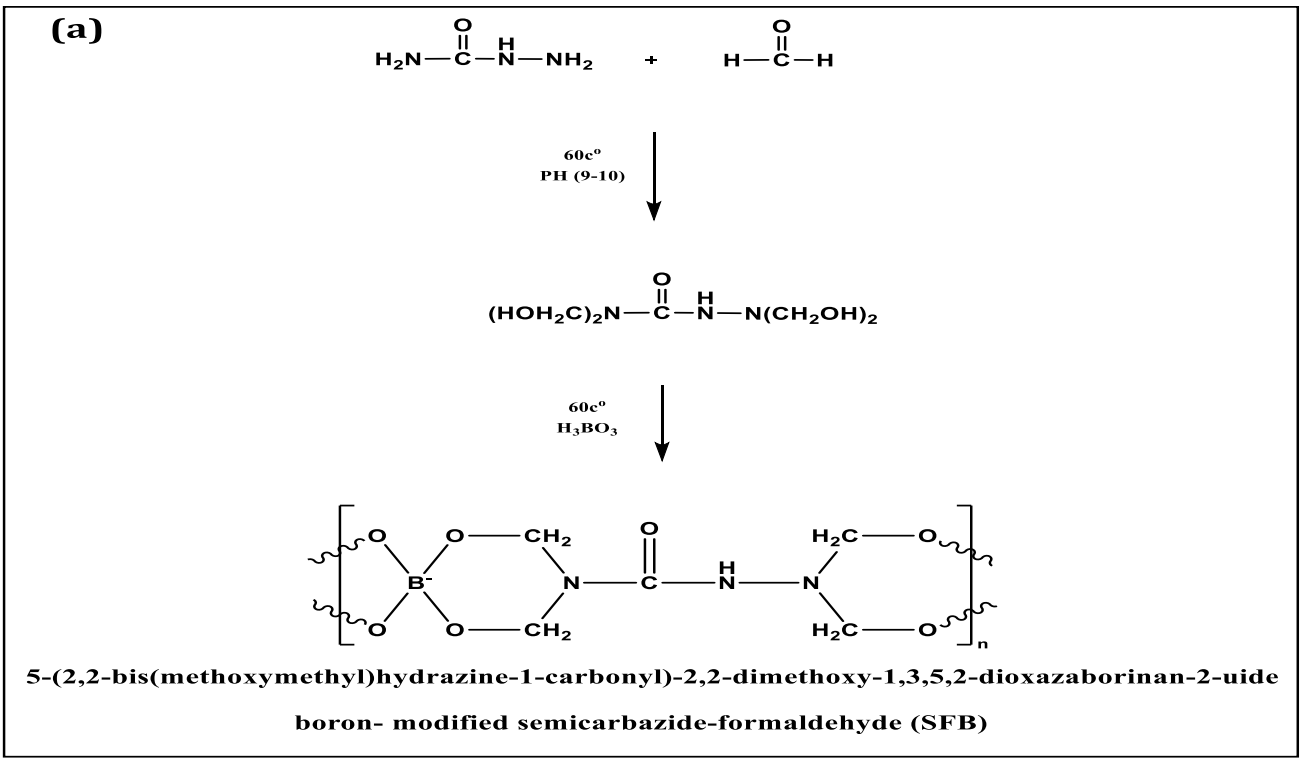

5-(2,2-bis(methoxymethyl)hydrazine-1-carbonyl)-2,2-dimethoxy-1,3,5,2-dioxazaborinan-2-uide

boron- modified semicarbazide-formaldehyde (SFB)

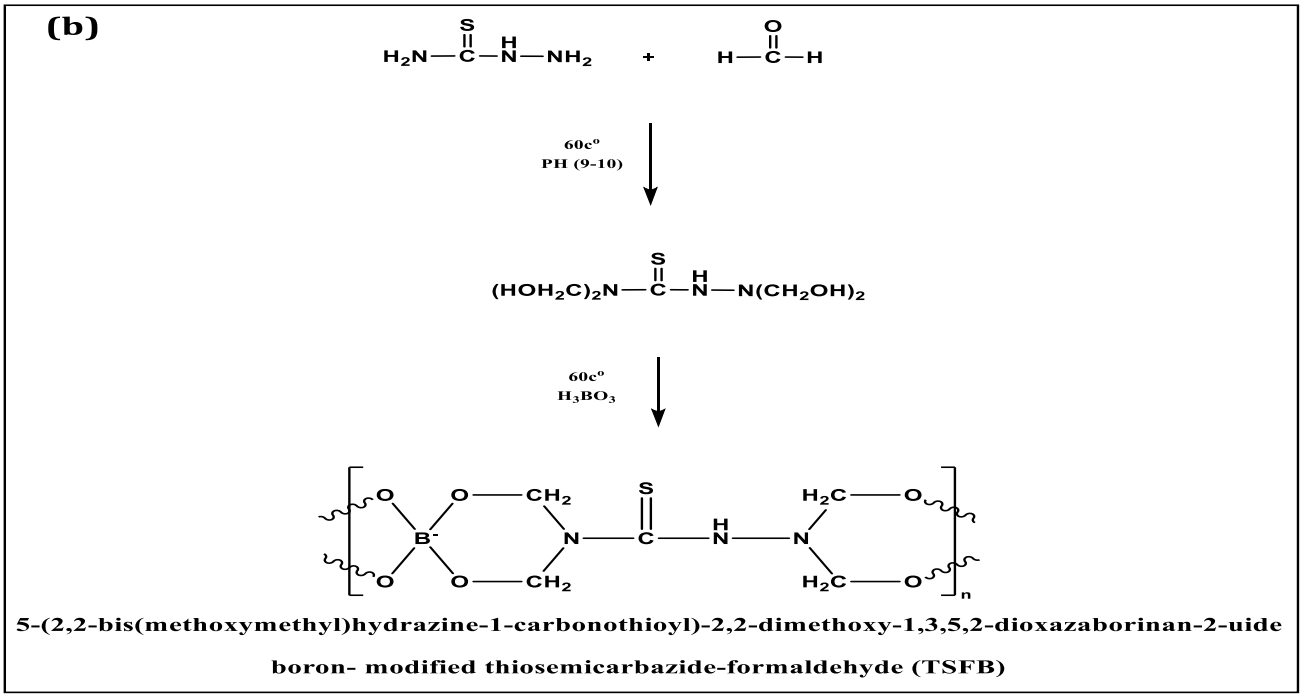

5-(2,2-bis(methoxymethyl)hydrazine-1-carbonothioyl)-2,2-dimethoxy-1,3,5,2-dioxazaborinan-2-uide

boron- modified thiosemicarbazide-formaldehyde (TSFB)

Fig. 1 *Scheme for the preparation of the resins (a) the preparation of boron containing semicarbazide-formaldehyde resin (SFB), (b) the preparation of boron containing thiosemicarbazide-formaldehyde resin (TSFB).*

Product characterization

The IR spectra of (SFB) as shown in Fig. 2 provide very informative data on the basis of stretching, bonds, twisting, and wagging of the various types of bonding, linkages, and functional groups present in the given polymer. Spectral study shows that, in the region 3321 cm^{-1} a broad band appears due to N-H groups interfering with hydroxyl groups, which exhibits an intermolecular hydrogen bonding with stretching vibration. The peaks at 2952 and 2900 cm^{-1} indicate the existence of $-CH_2$. The peak at 2358 cm^{-1} is assigned to the ($-C=N^+-H$) group [19]. The presence of a carbonyl group is further confirmed by the strong band displayed at 1651 cm^{-1}. The methylene bridges and $N-CH_2-N$ in the polymer chain are depicted in the region 1400-1446 cm^{-1}. The 1347 and 1515 cm^{-1} peaks are assigned to B-O-C and B-O-B, respectively [36]. The peak at 1100 cm^{-1} belongs to the C-O [20].

In Fig. 3, the important peaks in the FTIR spectrum for (TSFB) are revealed, where the 1382 and 1508 cm^{-1} peaks are assigned to B-O-C and B-O-B, respectively [36]. Furthermore, the adsorption in the region 3500-3600 cm^{-1} is assigned to the adsorption peak of the N-H. Peaks at 2932 and 2880 cm^{-1} indicate the existence of CH_2. The peak at 2358 cm^{-1} is assigned to the ($-C=N^+-H$) group. The peak at 1655 cm^{-1} can be attributed to the adsorption of C=S, and the peak at 1257 cm^{-1} shows C-N bond stretching. The peak at 1100 cm^{-1} belongs to the C-O. Therefore, the structure of the polymer can be confirmed by the FTIR spectrum [21].

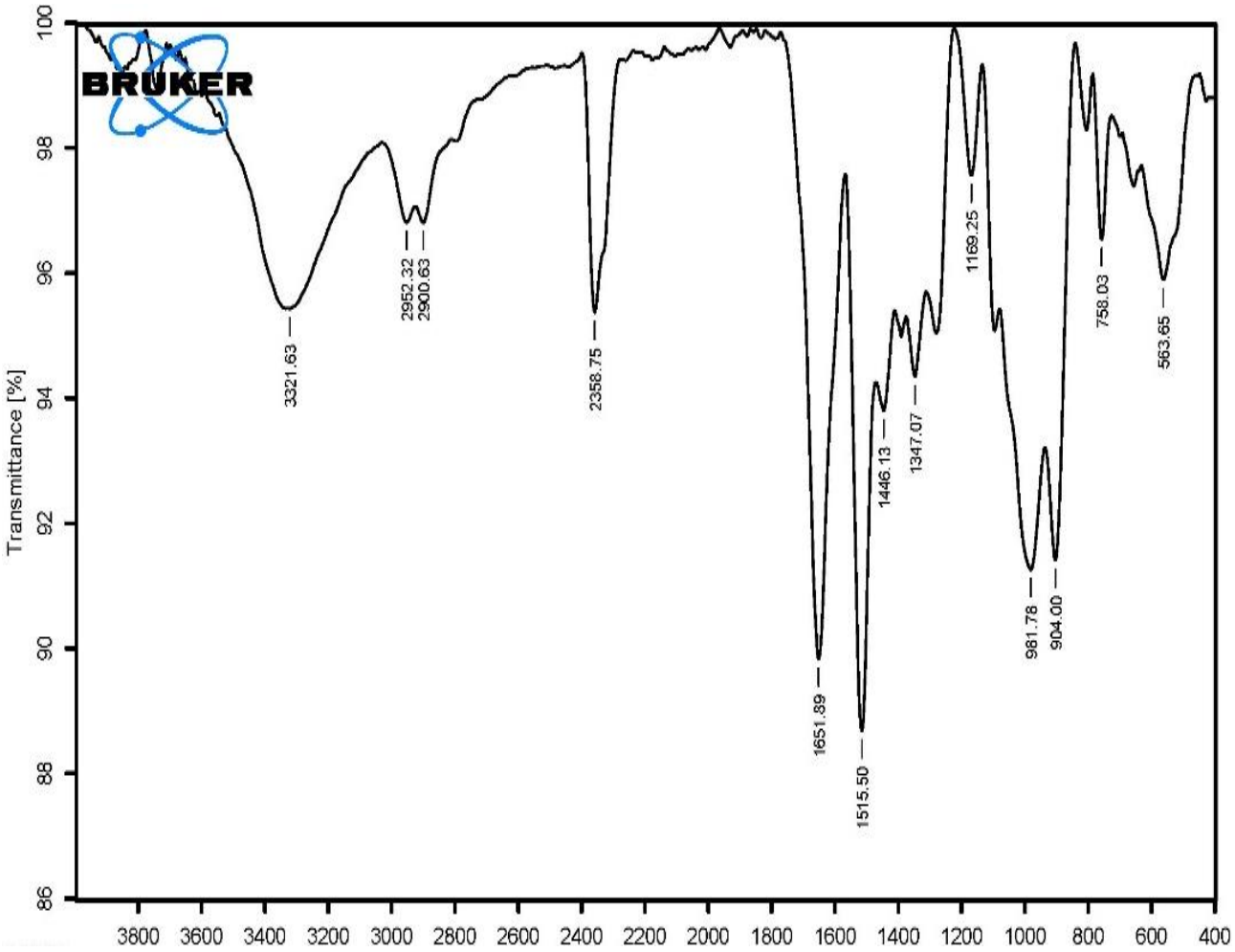

Fig. 2 *FTIR spectrum of boron containing semicarbazide-formaldehyde resin (SFB).*

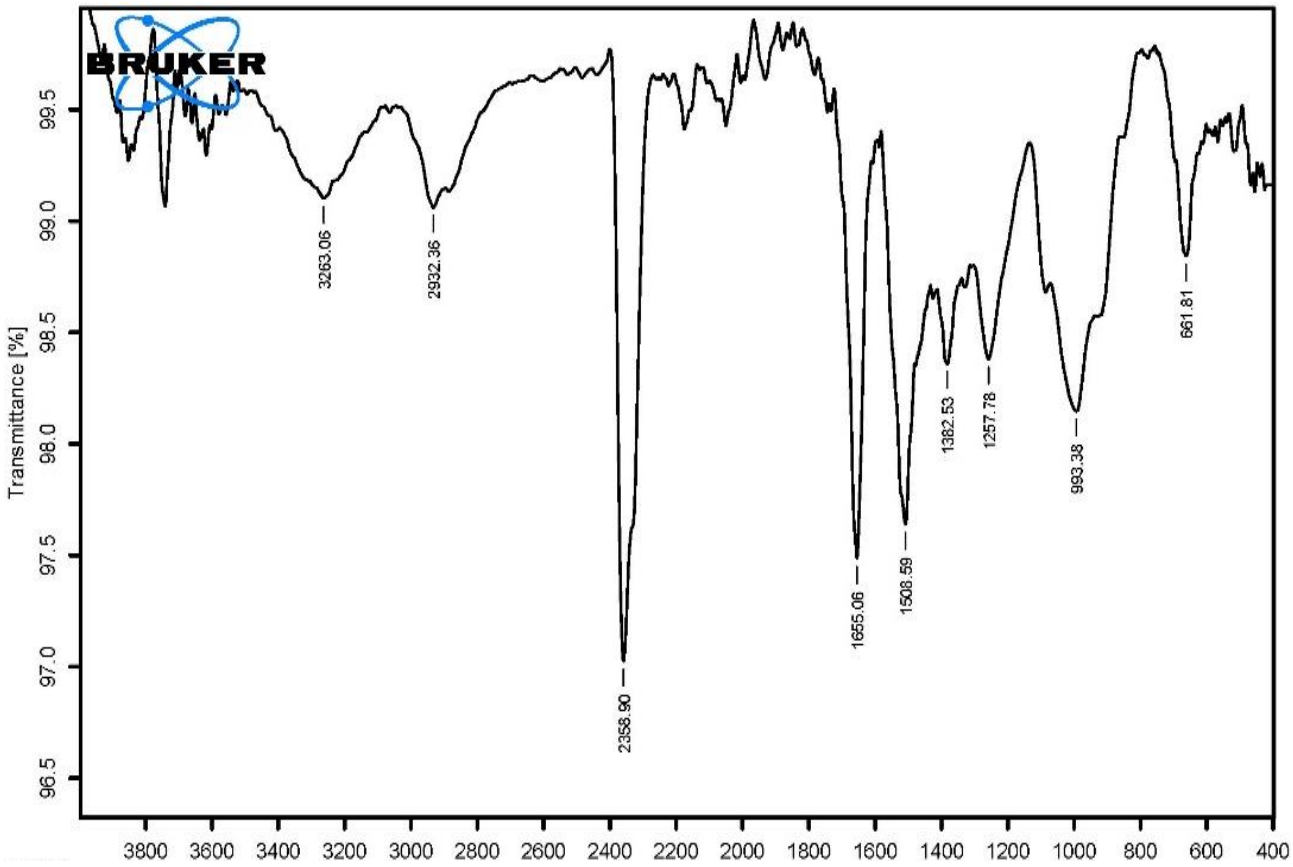

Fig. 3 *FTIR spectrum of boron containing thiosemicarbazide-formaldehyde resin (TSFB).*

Thermal Gravimetric Analysis (TGA)

Thermogravimetric analysis (TGA) was used to determine the weight loss behavior of the boron-containing semicarbazide or thiosemicarbazide formaldehyde cured resin. Degradation was performed in an inert atmosphere at a maximum temperature of 500 °C. The weight loss of the resin was calculated, and the weight loss rates are shown as a function of temperature in (Fig. 4, Fig. 5). The weight loss of the boron-containing thiosemicarbazide-formaldehyde resin was over 75% at (500 °C), and the residual weight at temperatures above (500 °C) was 25%. In contrast, the weight loss was only 60% for the boron-containing semicarbazide-formaldehyde resin, with a residual weight of 40% at temperatures above (550 °C). The TGA curves for thermal degradation show that both boron-containing resins degraded in two stages. In the first stage, weight loss was recorded at (225 °C) for the thiosemicarbazide resin, whereas it occurred at 275°C for the semicarbazide resin. In the second stage, starting at (310 °C) for the thiosemicarbazide resin and (320 °C) for the semicarbazide resin, the weight loss was 24%. Other result data are listed in (Table 1). These results show that the ultimate thermal degradation of the resins occurred with the cleavage of the B-O bond and demonstrated higher heat oxidation resistance [22].

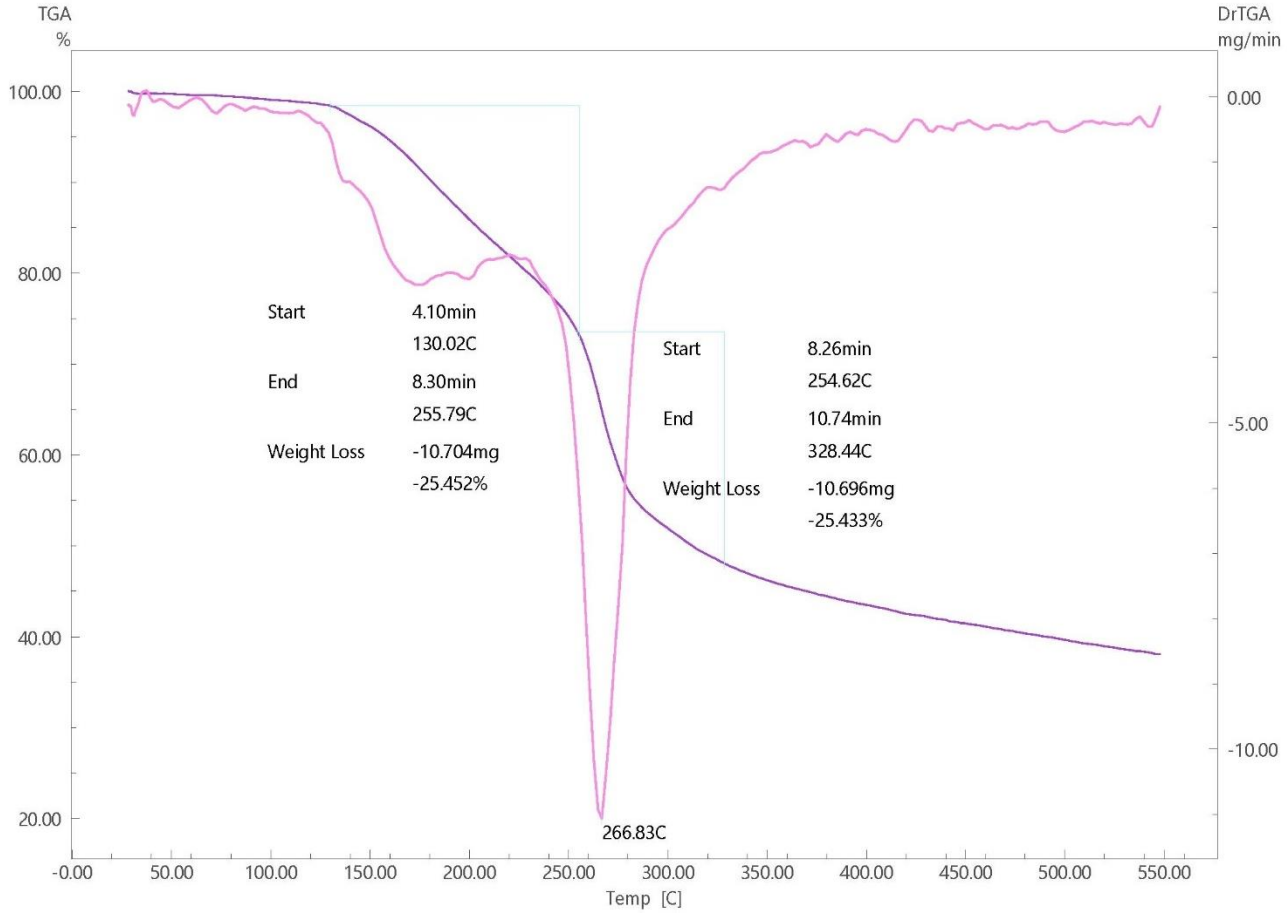

Fig. 4 *TGA of boron-containing semicarbazide-formaldehyde resin (SFB)*

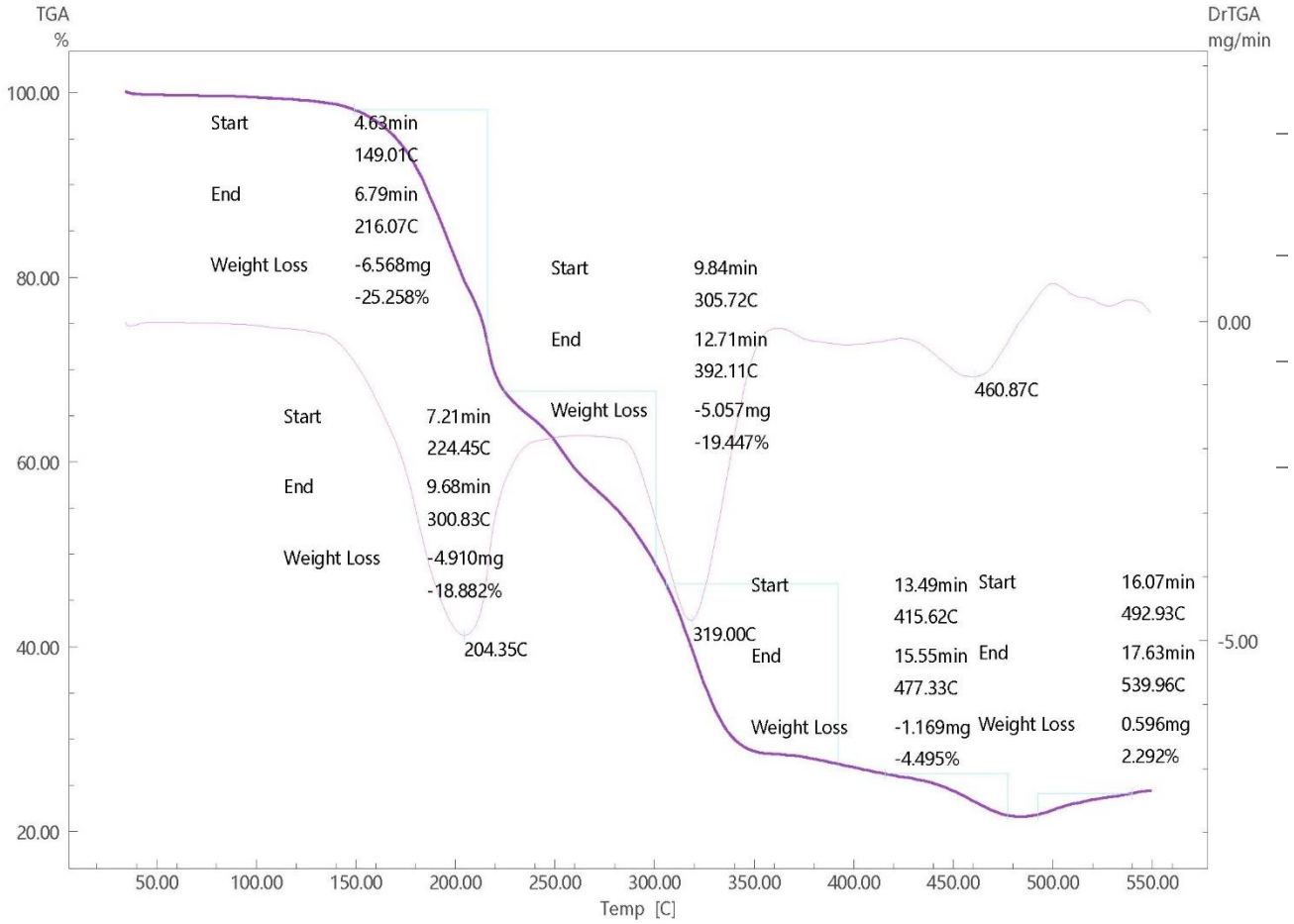

Fig. 5 *TGA of boron containing thiosemicarbazide-formaldehyde resin (TSFB).*

Table 1: Thermal weight loss (%) of (SFB) and (TSFB) at different temperatures.

Electrochemical analysis

The carbon steel alloy samples used in this study were provided by the Petroleum Pipelines Company affiliated with the Iraqi Ministry of Oil at the Khor Al-Zubair port site in Basra. Samples were taken from pipes used to transport oil products to sea tankers for export. The sample used in this study was examined and analyzed at Basra University/College of Engineering/Department of Mechanical Engineering to identify its components, and the results are shown in (Table 2).

Table 2: Composition of the carbon steel alloy.

C%	Si%	Mn%	P%	S%	Cr%	Mo%	Ni%	Al%	Cu%	V%	Fe%
0.097	0.31	1.10	0.003	0.002	0.027	0.007	0.20	0.036	0.032	0.037	98.0

Preparing the specimen

The examined carbon steel alloy models were taken and cut into circular disks with a diameter of 1.4 cm and a thickness of 2 mm. These dimensions were measured by the Vernier dimensional scale and washed with a 10% dilute hydrochloric acid solution to remove oxides. Then, it was washed with distilled water several times with ethanol and acetone, dried and kept in a dry place at room temperature. Subsequently, it was placed in the dried pot

(Desiccator), which contains silica gel to protect it from moisture. Using silicon carbide sheets of varying softness for smoothing samples. The smoothing process begins with No. 120, which is rough paper. Then, we continue smoothing using another type, No. 180, No. 400, No. 600, No. 1000, No. (2000), and finally No. (3000). Water is used for cooling during the softening process to prevent the temperature of the sample from rising and to prevent the grains of the softening paper from sticking to the surface of the sample, which affects the smoothness of the surface. The softening process is in one direction and perpendicular to the previous process. Every time the smoothing paper is changed, the sample is moved at an angle of 90° to remove the oxide layer covering the metal surface. Carbon steel models are washed and polished after the smoothing process. They are washed with soap and water to remove dirt and fat stuck in them, then washed again with distilled water and ethanol alcohol to remove the soap stuck in them, then immersed in acetone and dried with air. The specific pattern is then transferred to the polishing machine. It is placed on the rotating disc covered with a special type of shamwa smoothing fabric. The sample is moved in the direction of rotation of the disk with the addition of Al_2O_3 alumina powder. The pattern is then polished until it becomes shiny like a mirror free of any scratch. The model is washed again with distilled water, then ethanol alcohol, soaked in acetone, and dried in hot air. It is kept in a desiccator, which contains silica gel to protect it from moisture [23].

Results and Discussion

In this study, we assessed the effectiveness of boron-modified semicarbazide-formaldehyde (SFB) and boron-modified thiosemicarbazide-formaldehyde (TSFB) compounds as corrosion inhibitors. These assessments were conducted at temperatures of (298), (308), (318), and (328) K and varying concentrations within a (0.1 M) HCl corrosive medium. The evaluation used the Tafel plot extrapolation technique, operating at a sweep rate of (10 mV/sec). Comparative analyses of their performances are shown in Fig. 6 and Fig. 7, with the aggregated data presented in Table 3.

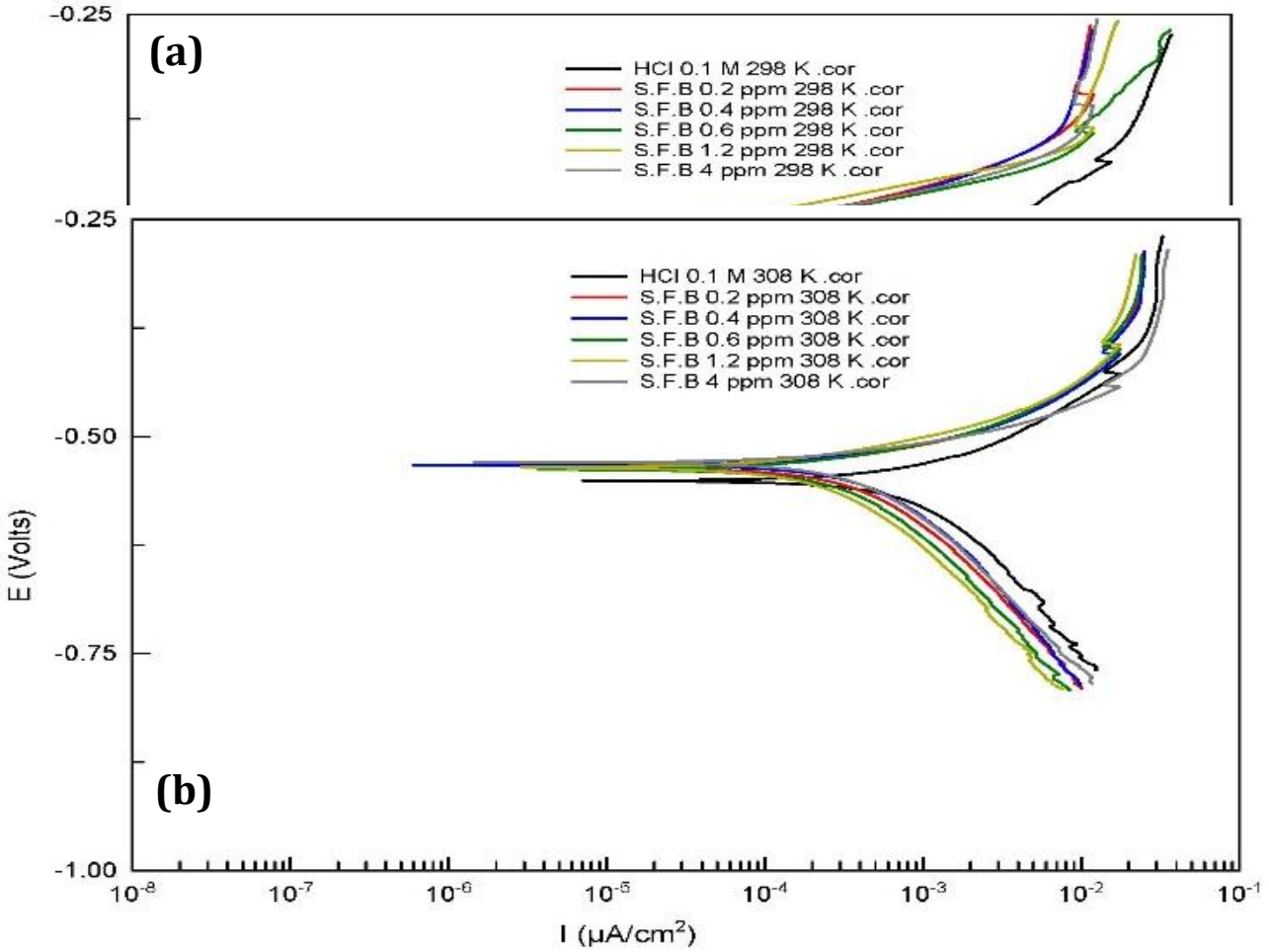

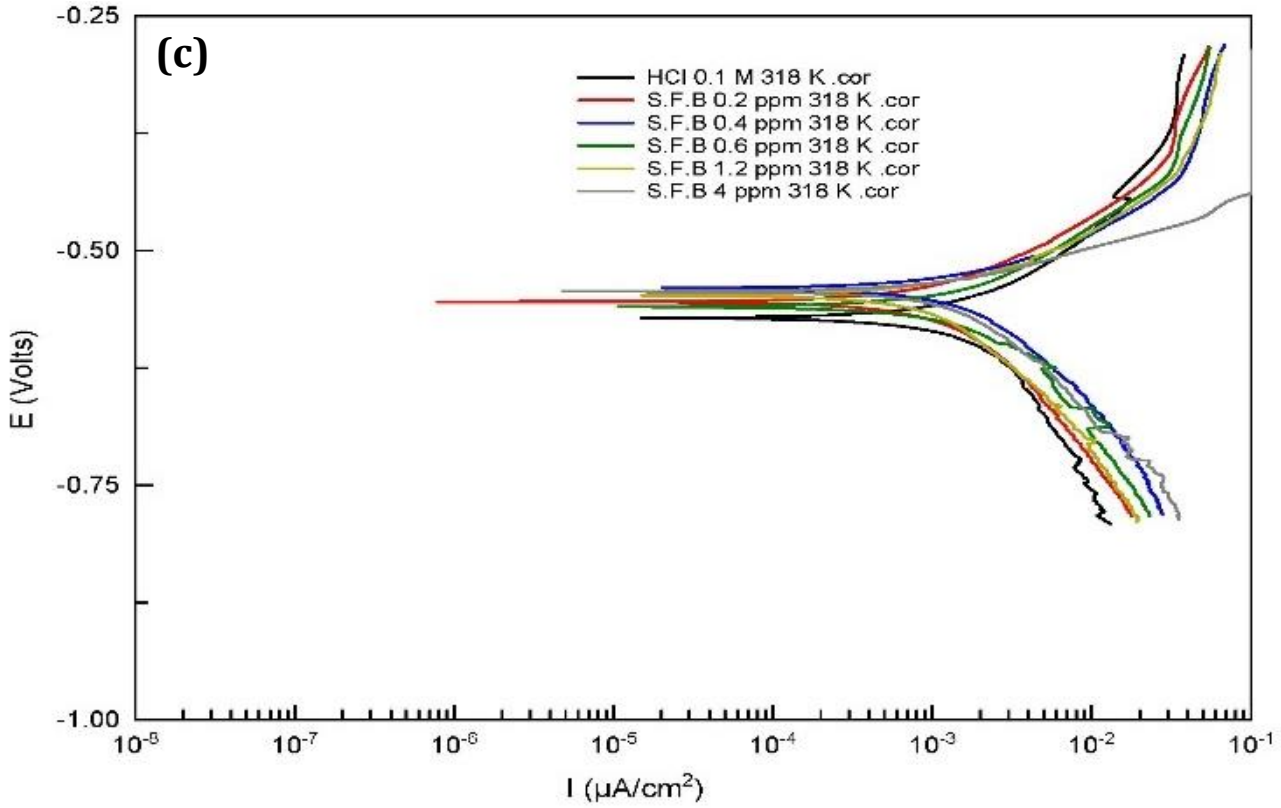

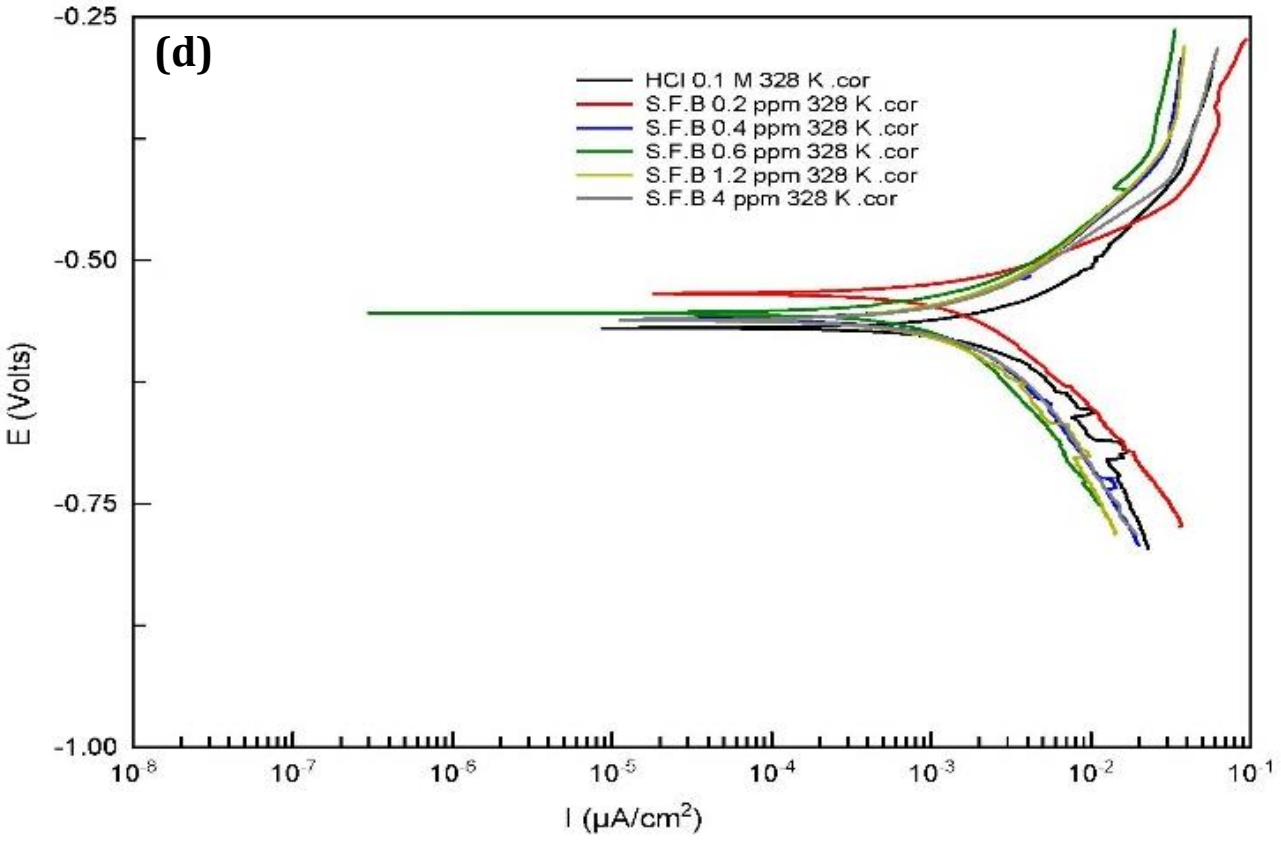

Fig. 6 *Tafel plot of the corrosion process occurring on the surface of carbon steel alloys in the presence of a corrosive environment and the effect of adding different concentrations of (SFB) at different temperatures: (a) 298 K, (b) 308 K, (c) 318 K, (d) 328 K.*

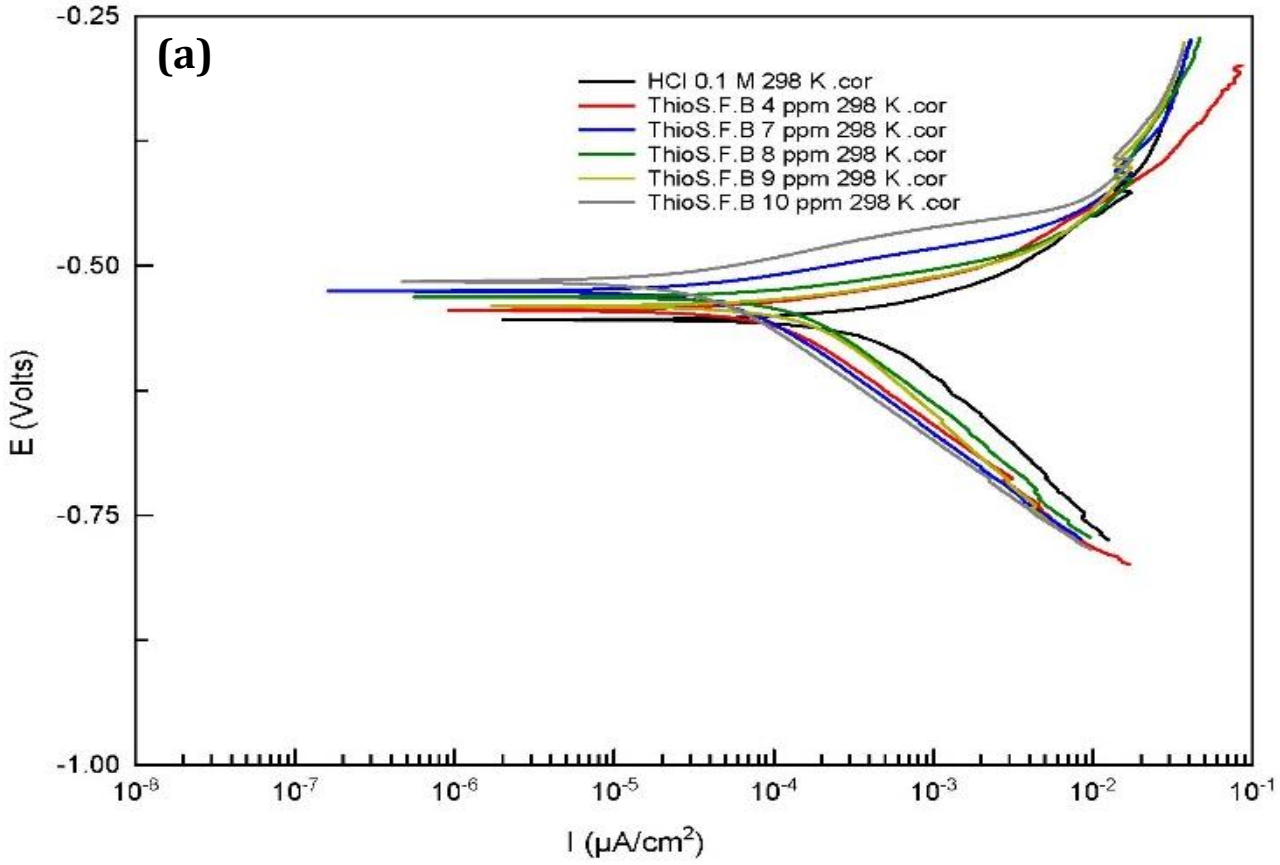
(a)
HCl 0.1 M 298 K .cor
ThioS.F.B 4 ppm 298 K .cor
ThioS.F.B 7 ppm 298 K .cor
ThioS.F.B 8 ppm 298 K .cor
ThioS.F.B 9 ppm 298 K .cor
ThioS.F.B 10 ppm 298 K .cor
E (Volts)
-0.25
-0.50
-0.75
-1.00
10-8
10-7
10-6
10-5
10-4
10-3
10-2
10-1
I (µA/cm2)

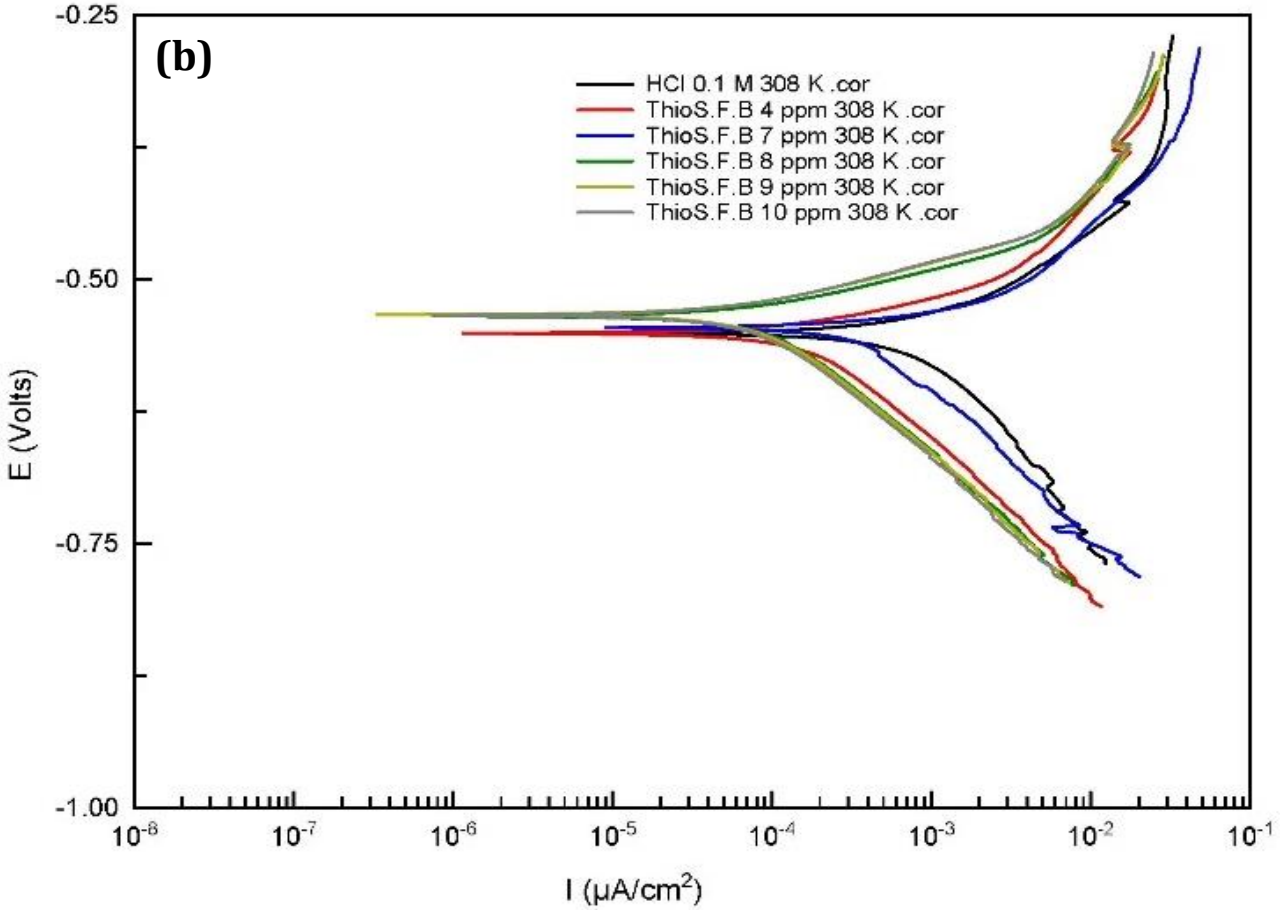
(b)
HCl 0.1 M 308 K .cor
ThioS.F.B 4 ppm 308 K .cor
ThioS.F.B 7 ppm 308 K .cor
ThioS.F.B 8 ppm 308 K .cor
ThioS.F.B 9 ppm 308 K .cor
ThioS.F.B 10 ppm 308 K .cor
E (Volts)
-0.25
-0.50
-0.75
-1.00
10-8
10-7
10-6
10-5
10-4
10-3
10-2
10-1
I (µA/cm2)

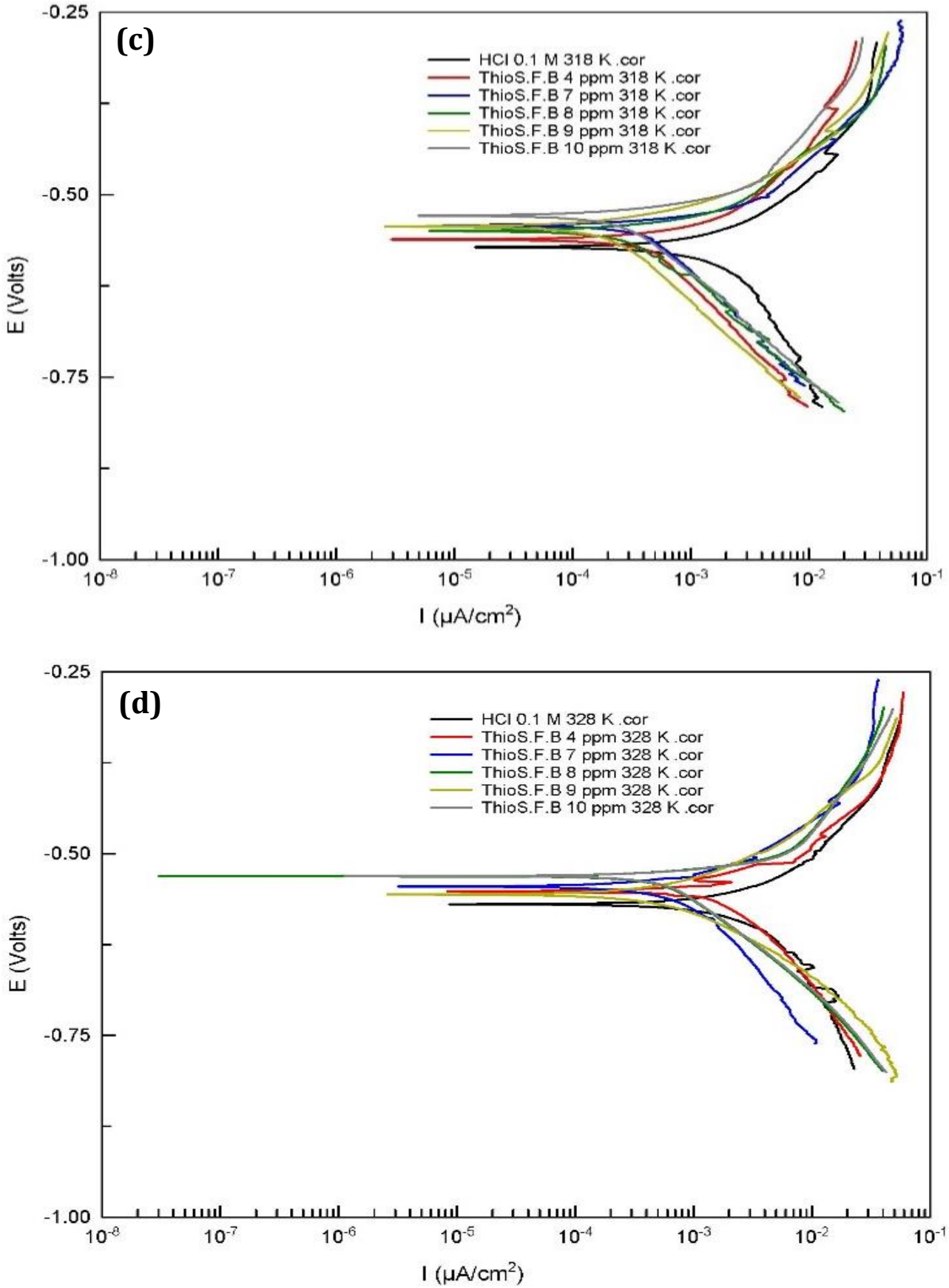

Fig. 7 *Tafel plot of the corrosion process occurring on the surface of carbon steel alloys in the presence of a corrosive environment and the effect of adding different concentrations of (TSFB) at different temperatures: (a) 298 K, (b) 308 K, (c) 318 K, (d) 328 K.*

Table 3 Data obtained from electrochemical experiments on the corrosion reaction of carbon steel in the presence of (SFB) and (TSFB) separately as corrosion inhibitors against 0.1 M HCl corrosive environment.

Conc. (ppm)	Temp. °C	$-E_{corr}$ (mV)	I_{corr} ($\mu A.cm^{-2}$)	CR (mpy)	β_a (mV/de.)	$-\beta_c$ (mV/de.)	Rp ($\Omega.cm^2$)	% IE	θ
0.1 M HCl corrosive environment									
Blank	25	554.24	773.00	358.02	97.36	222.96	35.93		
	35	550.95	1583.50	733.29	122.60	288.25	23.54		
	45	571.70	5805.90	2688.60	237.85	951.80	13.67		
	55	569.52	7421.90	3436.90	219.42	446.47	8.54		
After adding varying concentrations of (SFB)									
0.2	25	514.69	$1.05*10^{-4}$	48.91	66.22	168.95	210.64	86.3	0.86
	35	536.22	$6.74*10^{-4}$	312.38	94.035	254.56	45.621	57.4	0.57
	45	554.49	$1.84*10^{-3}$	852.08	120.21	231.51	18.467	68.3	0.68
	55	534.15	$2.89*10^{-3}$	1336	102.98	234.3	10.68	64.1	0.64
0.4	25	520.51	$9.77*10^{-5}$	45.25	67.87	191.15	239.5	87.4	0.87
	35	533.08	$8.05*10^{-4}$	372.92	98.566	275	39.447	49.1	0.49
	45	540.15	$3.06*10^{-3}$	1416.7	113.84	257.73	11.489	47.3	0.47
	55	560.59	$3.22*10^{-3}$	1491.6	173.54	308.93	14.566	56.6	0.56
0.6	25	523.11	$6.22*10^{-5}$	28.79	58.51	152.69	315.64	91.9	0.92
	35	538.06	$5.43*10^{-4}$	251.37	89.928	248.25	53.459	65.7	0.66
	45	559.93	$2.86*10^{-3}$	1313.6	139.49	226.33	12.839	51.1	0.51
	55	553.93	$2.17*10^{-3}$	1003.7	142.85	298.34	18.196	70.8	0.71
1.2	25	510.95	$5.43*10^{-5}$	25.12	57.47	169.59	374.43	92.9	0.93
	35	535.97	$3.58*10^{-4}$	165.71	80.317	203.32	74.069	77.4	0.77
	45	547.82	$2.08*10^{-3}$	963.03	104.97	281.07	15.014	64.2	0.64
	55	561.70	$2.58*10^{-3}$	1195	158.8	262.86	16.529	65.2	0.65
4	25	227.23	$1.73*10^{-15}$	$7.9*10^{-10}$	306.57	83.36	181.54	99.9	0.99
	35	530.35	$4.42*10^{-4}$	204.63	73.306	172.45	39.88	72.1	0.72
	45	543.61	$2.02*10^{-3}$	937.71	65.608	204.18	10.412	65.1	0.65
	55	561.49	$2.58*10^{-3}$	1194.9	135.99	244.85	14.195	65.2	0.65
After adding varying concentrations of (TSFB)									
4	25	739.03	$9.24*10^{-10}$	$4.3*10^{-4}$	56.917	-102.93	96.377	99.9	0.99
	35	551.14	$3.34*10^{-4}$	154.87	84.147	-208.67	74.224	78.9	0.79
	45	561.33	$1.71*10^{-3}$	792.99	148.67	-1179.4	25.61	70.5	0.70
	55	551.86	3.46*10-3	1602.4	135.79	-275.7	9.8527	53.4	0.53
7	25	525.93	$4.72*10^{-5}$	21.873	51.712	-104.92	213.99	93.9	0.94
	35	554.4	$1.57*10^{-4}$	72.657	71.928	98.215	22.523	90.1	0.90
	45	542.13	$1.24*10^{-3}$	574.32	105.21	-579.05	19.705	78.6	0.78
	55	545.06	$1.81*10^{-3}$	836.04	121.98	-393.88	20.462	75.7	0.76
8	25	981	$2.48*10^{-14}$	$1.2*10^{-8}$	59.178	-3354.4	73.522	99.9	0.99
	35	535.33	$1.45*10^{-4}$	67.256	66.571	-163.35	136.13	90.8	0.91
	45	549.83	$6.50*10^{-4}$	301.05	91.137	-222.43	30.803	88.8	0.89
	55	530.86	$1.09*10^{-3}$	505.44	98.165	-188.47	12.03	85.3	0.85
9	25	550.19	$2.13*10^{-5}$	9.8722	58.636	-91.155	69.617	97.2	0.97
	35	533.31	$1.23*10^{-4}$	56.976	63.686	-152.32	161.5	92.2	0.92
	45	543.87	$4.22*10^{-4}$	195.67	81.218	-276.56	55.435	92.7	0.93
	55	556.04	$9.84*10^{-4}$	455.94	104.83	-115.48	25.243	86.7	0.87
10	25	528.23	$1.92*10^{-6}$	0.88886	42.687	-69.654	355.29	99.7	0.99
	35	534.11	$1.16*10^{-4}$	53.747	64.364	-153.29	171.13	92.7	0.93
	45	532.97	$1.81*10^{-4}$	84.055	75.555	-113.06	32.625	96.9	0.97
	55	531.09	$3.51*10^{-4}$	162.43	72.451	-100.3	10.824	95.3	0.95

As indicated in Table 3, there was a reduction in both the corrosion current density and the corrosion rate in a 0.1 M HCl solution, whereas the resistance polarization increased with higher inhibitor concentrations. Conversely, the inhibitor efficiency and surface coverage

area, denoted by θ, remained largely unchanged as the inhibitor concentration increased at 298 K. This effect can be attributed to the (SFB) and (TSFB) inhibitor's capacity to adsorb onto the alloy's surface at the concentrations investigated [33]. Additionally, as Table 3 illustrates, the (E_{corr}) values explain a mixed inhibitor effect. This is evidenced by the fact that the variance in (E_{corr}) values at any given concentration when compared with those in a corrosive environment, is less than 85 mV [34,35]. The data from the anodic and cathodic Tafel values reveal that the inhibitor's effect is governed by the anodic dissolution of the alloy and the cathodic hydrogen evolution reaction. Moreover, an increase in temperature from 298 K to 328 K results in the desorption of inhibiting molecules from the carbon steel surface [28].

Adsorption isotherm

The inhibitory effects of the (SFB) and (TSFB) compounds were analyzed separately using various adsorption isotherm models, including Timken, Freundlich, Frumkin, and Langmuir, across a temperature spectrum of (25), (35), (45), and (55) °C. The Langmuir adsorption isotherm model demonstrated the closest fit to linear behavior at these temperatures, as indicated by the R^2 value nearing one [24]. The equation representing Langmuir's adsorption isotherm can be articulated as follows:

$$\frac{C}{\theta} = \frac{1}{K_{ads}} + C \qquad (1)$$

In this context, (C) denotes the concentration of the inhibitor measured in parts per million (ppm) or ($mg.L^{-1}$), θ represents the fraction of the surface covered, and K_{ads} is the equilibrium constant for adsorption in units of ($L.mg^{-1}$). The adsorption isotherms in (0.1) M HCl for different concentrations of (SFB) and (TSFB) are shown in Fig. 6 , Fig.7, and Table 4.

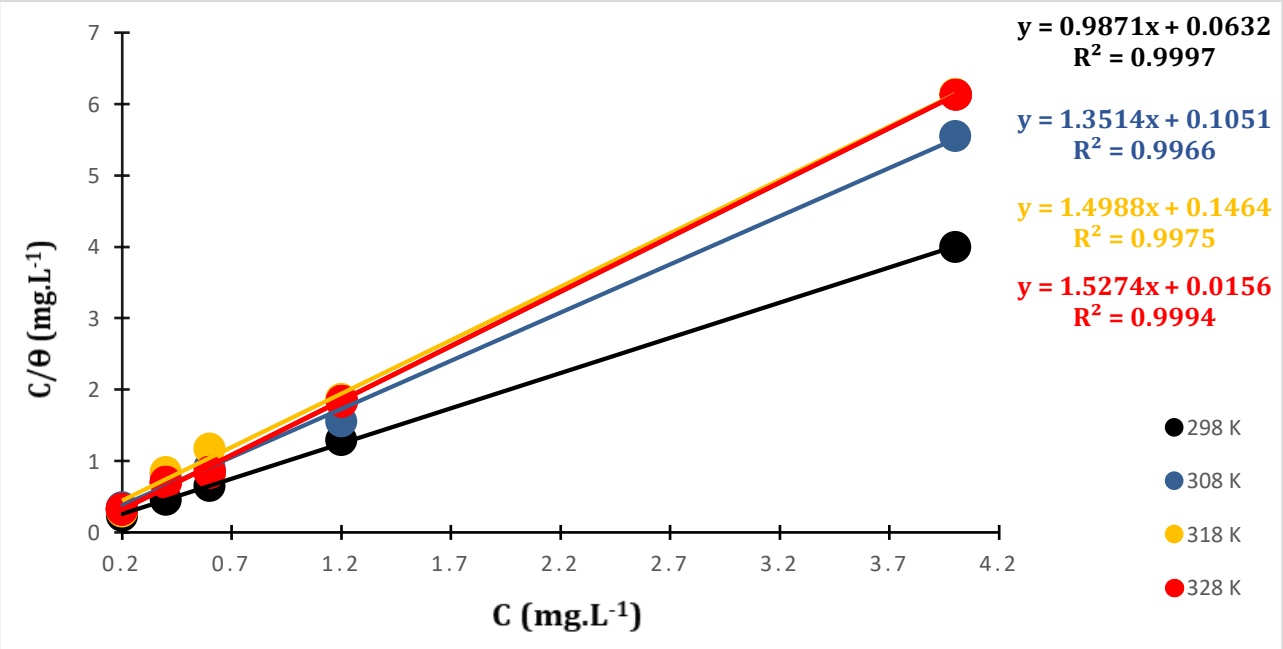

Fig. 6 Langmuir adsorption isotherm of (SFB) on carbon steel surfaces at different temperatures.

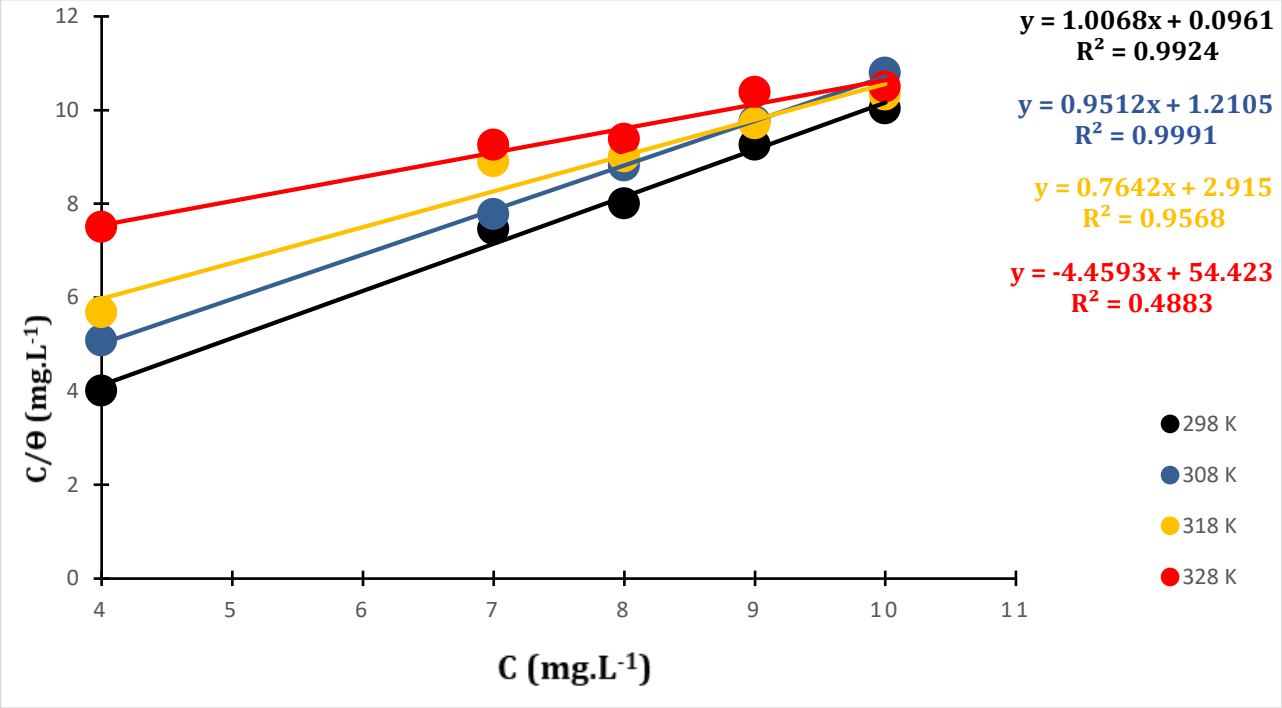

Fig. 7 *Langmuir adsorption isotherm of (TSFB) on carbon steel surfaces at different temperatures.*

The Gibbs free energy of adsorption, denoted as ΔG°_{ads} , is determined by the following equation:

$$\Delta G^{\circ}_{ads} = -RT \ln 55.5\, K_{asd} \qquad (2)$$

The precise concentration of the inhibitor in this study, expressed in mg.L^{-1} (ppm), when applied to equation (3) can be reformulated as follows:

$$\Delta G^{\circ}_{ads} = -RT \ln 999000\, K_{asd} \qquad (3)$$

The value of 999000 corresponds to the conversion of water molecules from 55.5 (mol.L^{-1}) to (mg.L^{-1}) which facilitates the expression of inhibitor concentrations in mg.L^{-1} (ppm) [25]. Here, (R) stands for the universal gas constant, valued at ($8.314\, J.K^{-1}.mol^{-1}$), and (T) signifies the absolute temperature. The enthalpy of adsorption, ΔH°_{ads} can be deduced using the Gibbs-Helmholtz equation as follows:

$$\frac{\Delta G^{\circ}_{ads}}{T} = \frac{\Delta H^{\circ}_{ads}}{T} + k \qquad (4)$$

In this case, (k) is the constant that denotes the entropy of adsorption, ΔS°_{ads} . The thermodynamic calculations are concisely presented in Table 4, while the computation of ΔH°_{ads} and ΔS°_{ads} is elucidated in Fig. 8 and Fig. 9.

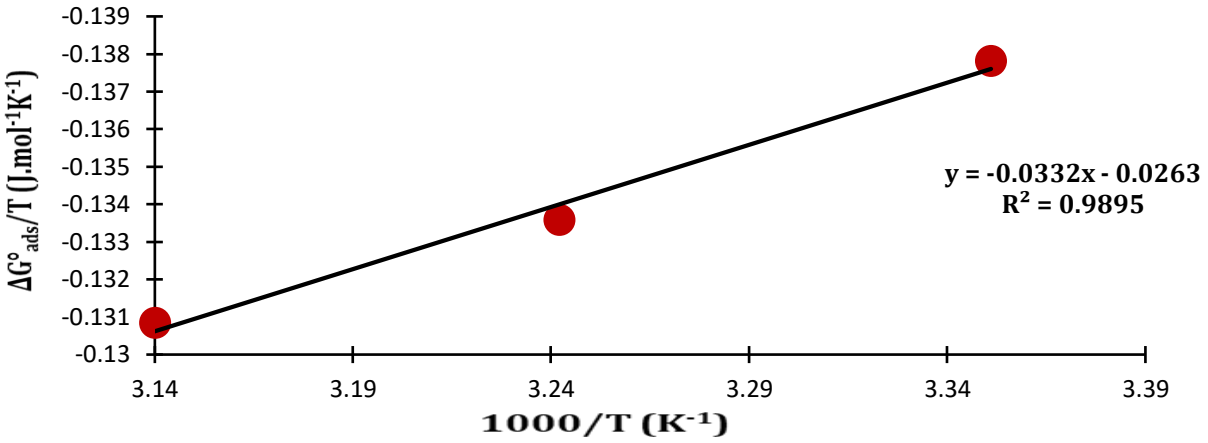

Fig. 8 Enthalpy and entropy computation of the adsorption of (SFB) as inhibitor on the surface of the alloy.

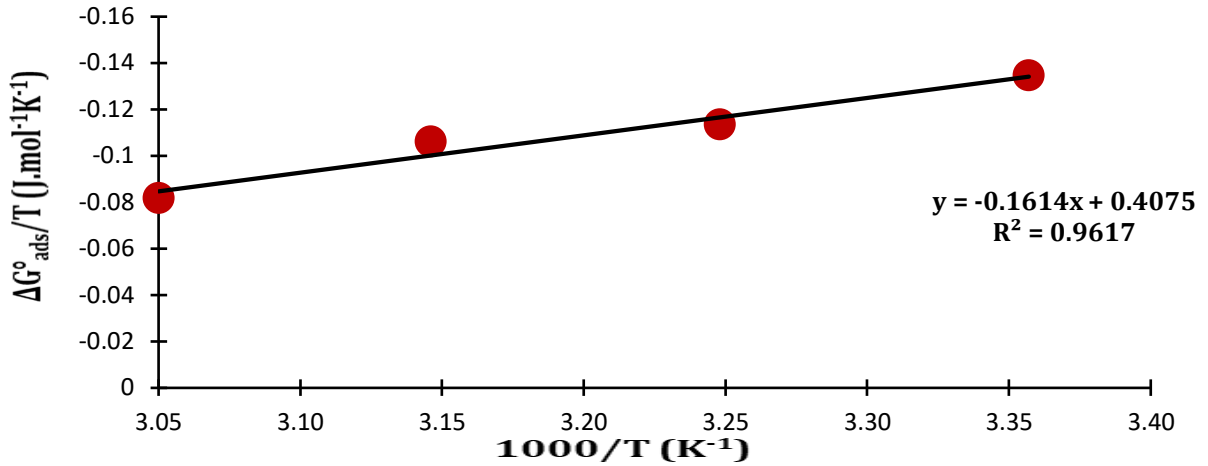

Fig. 9 *Enthalpy and entropy computation of the adsorption of (TSFB) as inhibitor on the surface of the alloy.*

Table 4: Thermodynamic function of the adsorption of (SFB) and (TSFB)on the surface of the alloy.

Comp.	K_{asd} ($L.mg^{-1}$)	R^2	ΔG°_{ads} ($kJ.mol^{-1}$)	ΔH°_{ads} ($kJ.mol^{-1}$)	ΔS°_{ads} ($J.K^{-1}.mol^{-1}$)	Temp. °c
SFB	15.823	0.9997	-41.068	-0.0332	-0.0263	25
	9.515	0.9966	-41.143			35
	6.831	0.9975	-41.603			45
	64.103	0.9994	-49.017			55
TSFB	10.406	0.9924	-40.029	-0.1614	0.4075	25
	0.826	0.9991	-34.885			35
	0.343	0.9568	-33.694			45
	0.183	0.4883	-26.772			55

According to Table 4, the Gibbs free energy for both (SFB) and (TSFB) values are spontaneous and are reduced as the temperature is increased. Furthermore, the enthalpy of adsorption values for (SFB) and (TSFB) are negative, which reveals very little exothermic behavior, especially for (SFB), which insists that a physical behave for mode of adsorption [26]. On the other hand, the entropy are negative values is reduced as temperature increased, which means the entropy is raised as temperature reduced, where the corrosive molecules

and corrosion inhibitor molecules tend to be competitive to adsorbed on the surface of alloy [27].

Kinetic parameter calculations

In this study, we determined the kinetic parameters, including activation energy (E_a), activation enthalpy (ΔH^*), activation entropy (ΔS^*) and activation Gibbs free energy (ΔG^*) for the corrosion reaction on the alloy surface. These calculations were performed at three distinct SFB concentrations (0.2, 0.4, and 1.2 ppm) and distinct TSFB concentrations (7, 9, and 10 ppm) compared to scenarios without the inhibitor. The selection of these specific concentrations was based on their association with the most favorable R^2 values. Initially, we employed the Arrhenius equation to calculate the activation energy (E_a), as illustrated below [27]:

$$\ln CR = \ln A - \frac{E_a}{RT} \qquad (5)$$

In this context, CR represents the corrosion rate, A stands for the pre-exponential factor in the Arrhenius equation, and T denotes the absolute temperature. By plotting the natural logarithm of CR (ln CR) against the reciprocal of the temperature ($\frac{1}{T}$), as illustrated in Fig. 10 and Fig. 11, the resulting slope is the ratio of the activation energy (E_a) to the gas constant ($\frac{E_a}{R}$).

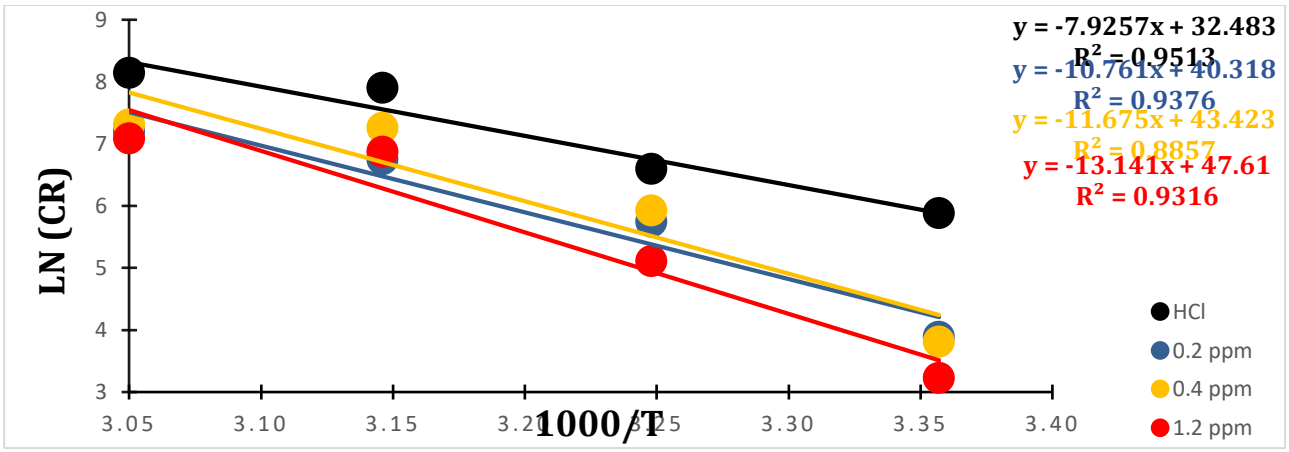

Fig. 10 Arrhenius relationship plot for the corrosion reaction of carbon steel in a corrosive environment with varying SFB concentrations acting as inhibitors.

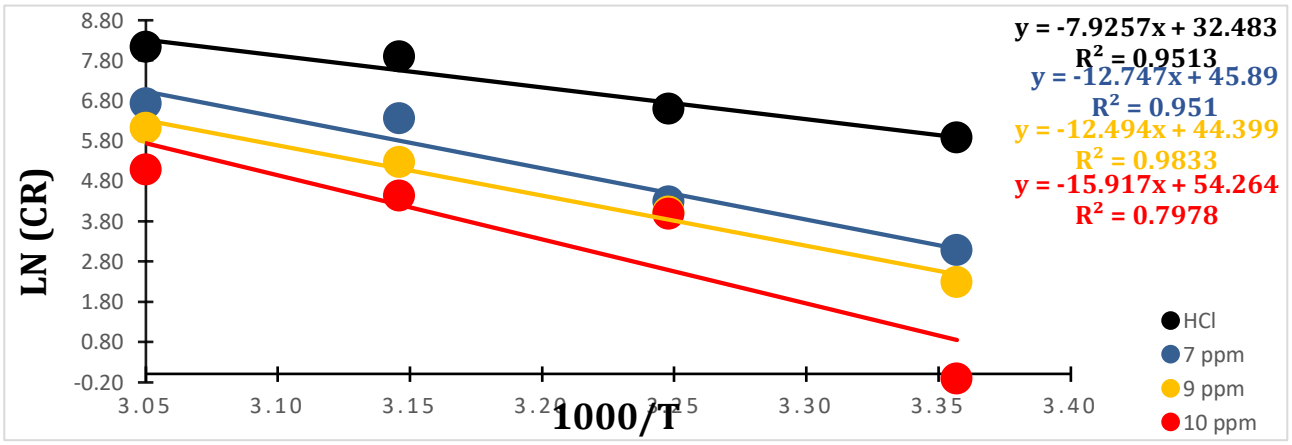

Fig. 11 Arrhenius relationship plot for the corrosion reaction of carbon steel in a corrosive environment with varying TSFB concentrations acting as inhibitors.

We use the following equation to determine the activation enthalpy and activation entropy [27]:

$$\ln\frac{CR}{T} = [\ln\frac{R}{Nh} + \frac{\Delta S^*}{R}] - \frac{\Delta H^*}{RT} \qquad (6)$$

where N is Avogadro's number $N = 6.023 \times 10^{23} mol^{-1}$& h is Planck's constant $h = 6.625 \times 10^{-34} J.s$. By plotting $\ln\frac{CR}{T}$ against $\frac{1}{T}$, the slope is $\frac{-\Delta H^*}{R}$ and the intercept is $[\ln\frac{R}{Nh} + \frac{\Delta S^*}{R}]$.

Figures 12 and 13 demonstrate how activation enthalpy and activation entropy are calculated when SFB and TSFB are used as inhibitors in a corrosive environment.

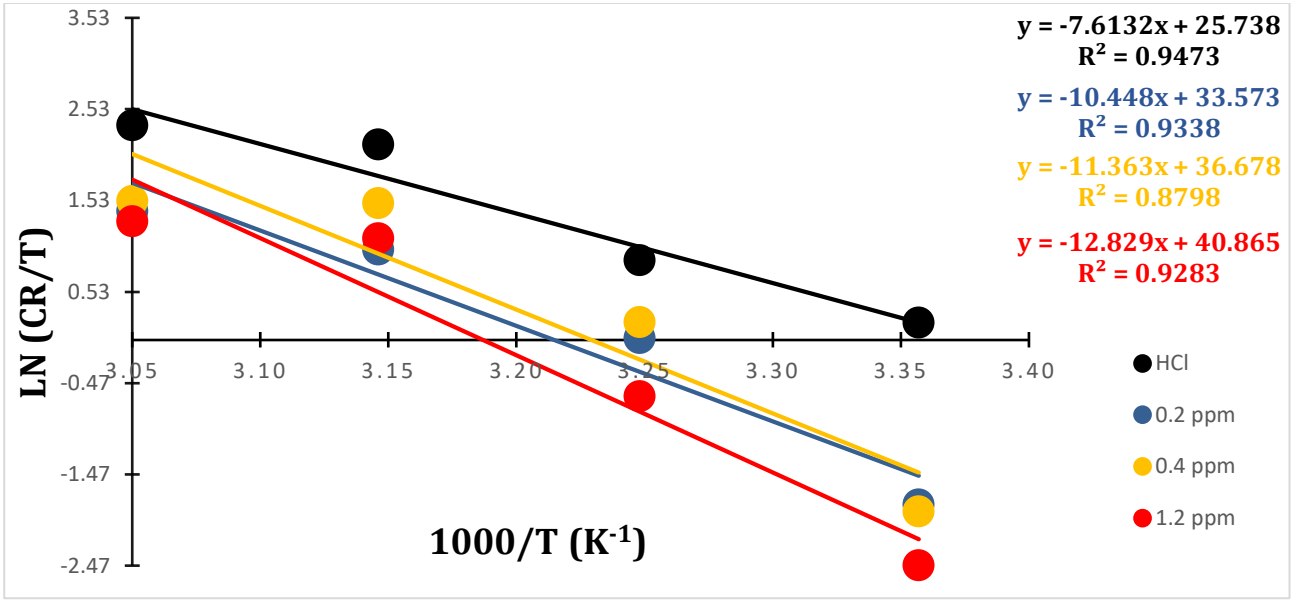

Fig. 12 Enthalpy of activation calculations for carbon steel corrosion reaction when various concentrations of SFB are present as inhibitors relative to the corrosive environment.

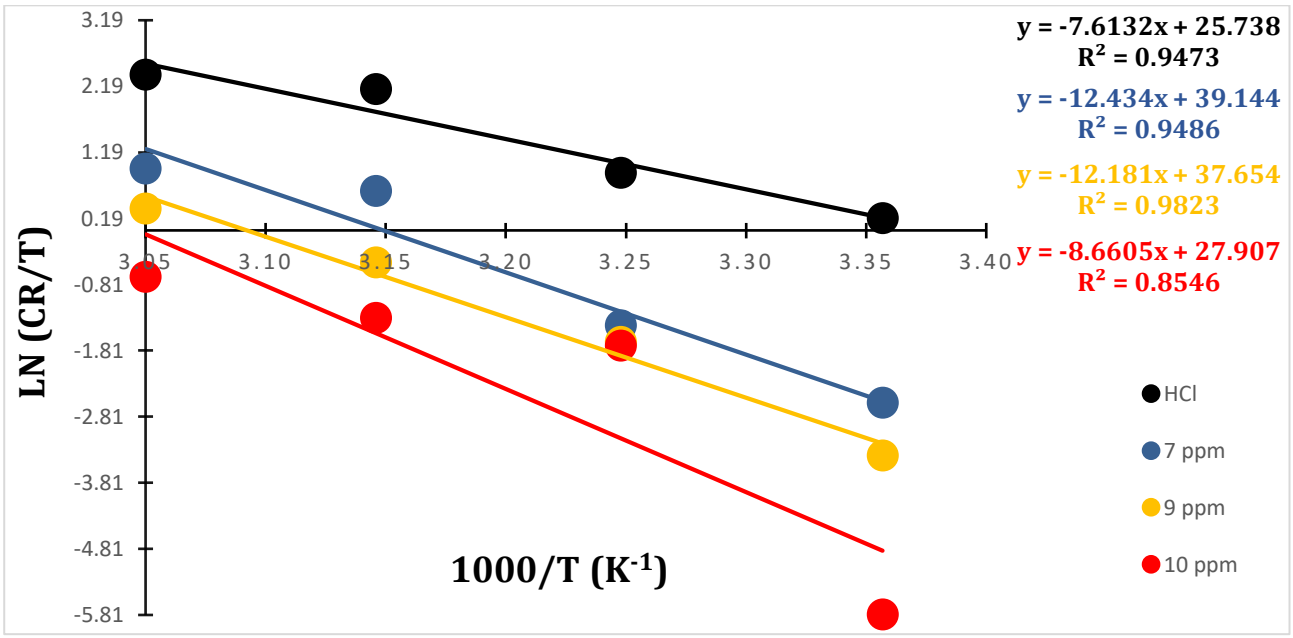

Fig. 13 Enthalpy of activation calculations for carbon steel corrosion reaction when various concentrations of TSFB are present as inhibitors relative to the corrosive environment.

Table 5 Kinetic factors of the corrosion reaction on alloy surfaces with and without inhibitors

Comp.	Conc. ppm	A (s^{-1})	E_a ($kJ.mol^{-1}$)	R^2	ΔH^* ($kJ.mol^{-1}$)	ΔS^* ($J.K^1.mol^{-1}$)	R^2
Blank	-	1.28×10^{14}	65.894	0.9513	63.296	16.446	0.9473
SFB	0.2	3.24×10^{17}	89.467	0.9376	86.865	81.586	0.9338
SFB	0.4	7.22×10^{18}	97.066	0.8857	94.472	107.40	0.8798
SFB	1.2	4.75×10^{20}	109.254	0.9316	106.66	142.21	0.9283
TSFB	7	8.51×10^{19}	105.979	0.9510	103.38	127.90	0.9486
TSFB	9	1.92×10^{19}	103.875	0.9833	99.153	115.52	0.9823
TSFB	10	3.69×10^{23}	132.334	0.7978	72.003	34.479	0.8546

(SFB) or (TSFB).

It is noted from Table 5 that the activation energy (E_a) is higher in the presence of the inhibitors, which means that the corrosion reaction of the carbon steel iron alloy is faster in the absence of the inhibitor, but in the presence of the inhibitor, the activation energy increases, which leads to the interaction of the inhibitor with the surface of the alloy and the formation of a protective layer on the surface of the alloy. This effect can be insisted upon by increasing the Arrhenius pre-exponential factor (A) when the inhibitor is present, leading to intensified vibrations of the inhibitor molecules on the alloy surface. As a result, the presence of inhibitors, in contrast to their absence, increases the levels of entropy activation [30]. On the other hand, the enthalpy of activation (ΔH^*) for the corrosion reaction is observed to have positive values, meaning that the alloy corrosion reaction increases in the presence or absence of the inhibitor with increasing temperature, and it corresponds to a decrease in the inhibition efficiency with increasing temperature [31]. The activation entropy (ΔS^*) values are positive. This indicates that the entropy of the products is greater than that of the reactants, meaning that the process of adsorption of the inhibitor causes great randomness that affects the corrosion reaction, ending with the expulsion of most of the corrosive molecules along with the water molecules, leading to the formation of an adsorbent layer that reduces the corrosion process [32].

Conclusion:

Innovative polymers have been synthesized from boron-altered semicarbazide formaldehyde (SFB) and boron-altered thiosemicarbazide formaldehyde (TSFB). The focus of this study was on the anti-corrosion characteristics of these polymers and how the corrosion rate of a carbon steel alloy is affected by the time of synthesis, the temperature of the reaction, and the molar ratios of the elements in a hydrochloric acid solution with inhibitors. The research showed that the inhibitors are highly effective, with (SFB) achieving efficiency rates of 86.3%, 87.4%, 91.9%, 92.9%, and 99.9% at concentrations of 0.2, 0.4, 0.6, 1.2, and 4 ppm, respectively. (TSFB) showed efficiencies of 99.9%, 93.9%, 99.9%, 97.2%, and 99.7% at concentrations of 4, 7, 8, 9, and 10 ppm, respectively, indicating that increases in the concentration did not significantly impact the efficiency. However, as the temperature was increased from 25 °C to 55 °C, the effectiveness of both inhibitors decreased because of the

disintegration of the inhibitor coating, which left the alloy exposed to corrosion. Thermodynamic adsorption functions confirmed these findings, showing a decrease in spontaneous adsorption with increasing temperature. In addition, kinetic parameters like the enthalpy of activation indicated an endothermic reaction for corrosion, suggesting that the corrosion process is accelerated by higher temperatures, thus diminishing the inhibitors' efficiency. Conversely, inhibitor adsorption exhibits mixed inhibition characteristics. The activation entropy remains positive in both the presence and absence of the inhibitor; however, it increases with the inhibitor because of the heightened kinetic energy of the inhibitor molecules during adsorption onto the alloy surface. This increase is evidenced by the elevated Arrhenius pre-exponential values when inhibitors are present, compared with the absence of inhibitors.

References

1. Vasechkina, I. A., Gladchenkova, Y. S., & Amezhnov, A. V. (2023). Effect of pipe steel chemical composition and structural characteristics on corrosion resistance under Western Siberia oilfield pipeline operating conditions. Metallurgist, 67(5–6), 579–589. https://doi.org/10.1007/s11015-023-01546-9
2. Natarajan, K. A. (2020). Principles of Corrosion Processes. Structural Integrity, 27–82. https://doi.org/10.1007/978-3-030-32831-3_2
3. Jellesen, M. S. (2018). Metals and corrosion. Metal Allergy, 17–22. https://doi.org/10.1007/978-3-319-58503-1_2
4. Ma, I. A., Ammar, Sh., Kumar, S. S., Ramesh, K., & Ramesh, S. (2021). A concise review on corrosion inhibitors: Types, mechanisms and electrochemical evaluation studies. Journal of Coatings Technology and Research, 19(1), 241–268. https://doi.org/10.1007/s11998-021-00547-0
5. Ahmed, S. K., Ali, W. B., & Khadom, A. A. (2019). Synthesis and investigations of heterocyclic compounds as corrosion inhibitors for mild steel in hydrochloric acid. International Journal of Industrial Chemistry, 10(2), 159–173. https://doi.org/10.1007/s40090-019-0181-8
6. Ates, M. (2016). A review on conducting polymer coatings for corrosion protection. Journal of Adhesion Science and Technology, 30(14), 1510–1536. https://doi.org/10.1080/01694243.2016.1150662
7. Xu, H., & Zhang, Y. (2019). A review on conducting polymers and nanopolymer composite coatings for steel corrosion protection. Coatings, 9(12), 807. https://doi.org/10.3390/coatings9120807
8. Ide, Y., Manabe, Y., Inaba, Y., Kinoshita, Y., Pirillo, J., Hijikata, Y., Yoneda, T., Shivakumar, K. I., Tanaka, S., Asakawa, H., & Inokuma, Y. (2022). Determination of the critical chain length for macromolecular crystallization using structurally flexible polyketones. Chemical Science, 13(34), 9848–9854. https://doi.org/10.1039/d2sc03083g
9. Tiu, B. D., & Advincula, R. C. (2015). Polymeric corrosion inhibitors for the oil and gas industry: Design principles and mechanism. Reactive and Functional Polymers, 95, 25–45. https://doi.org/10.1016/j.reactfunctpolym.2015.08.006
10. Fekry, A. M., & Mohamed, R. R. (2010). Acetyl thiourea chitosan as an eco-friendly inhibitor for mild steel in sulphuric acid medium. Electrochimica Acta, 55(6), 1933–1939. https://doi.org/10.1016/j.electacta.2009.11.011

11. Gharbi, O., Thomas, S., Smith, C., & Birbilis, N. (2018). Chromate replacement: What does the future hold? Npj Materials Degradation, 2(1). https://doi.org/10.1038/s41529-018-0034-5
12. Serdaroğlu, G., & Kaya, S. (2021). Organic and inorganic corrosion inhibitors. Organic Corrosion Inhibitors, 59–73. https://doi.org/10.1002/9781119794516.ch4
13. Tang, Z. (2019). A review of corrosion inhibitors for rust preventative fluids. Current Opinion in Solid State and Materials Science, 23(4), 100759. https://doi.org/10.1016/j.cossms.2019.06.003
14. Ress, J., Martin, U., & Bastidas, D. M. (2021). Improved corrosion protection of acrylic waterborne coating by doping with microencapsulated corrosion inhibitors. Coatings, 11(9), 1134. https://doi.org/10.3390/coatings11091134
15. Moses, Joseph & Chinweike, Ekenyem & Imah, Adindu. (2019). Evaluating the inhibitive synergy of di-anodic inhibitors in abatement of low carbon steel corrosion in cooling water systems. 4. 67-72. https://doi.org/10.36713/epra2016
16. Yi, X., Feng, A., Shao, W., & Xiao, Z. (2015). Synthesis and properties of graphene oxide–boron-modified phenolic resin composites. High Performance Polymers, 28(5), 505–517. https://doi.org/10.1177/0954008315587953
17. Patel, K. D., Desai, D. J., Morekar, M. M., & Tilak, Y. S. (2004). Synthesis, characterization and glass - reinforced composites of thiourea - formaldehyde - phenol resin. E-Journal of Chemistry, 1(5), 256–262. https://doi.org/10.1155/2004/569824
18. Nagieb, Z. A., Nassar, M. A., & El-Meligy, M. G. (2011). Effect of addition of boric acid and borax on fire-retardant and mechanical properties of urea formaldehyde saw Dust Composites. International Journal of Carbohydrate Chemistry, 2011, 1–6. https://doi.org/10.1155/2011/146763
19. Xiong, Y., Wan, L., Xuan, J., Wang, Y., Xing, Z., Shan, W., & Lou, Z. (2016). Selective recovery of ag(i) coordination anion from simulate nickel electrolyte using corn stalk based adsorbent modified by ammonia–thiosemicarbazide. Journal of Hazardous Materials, 301, 277–285. https://doi.org/10.1016/j.jhazmat.2015.09.003
20. Yi, X., Feng, A., Shao, W., & Xiao, Z. (2015). Synthesis and properties of graphene oxide–boron-modified phenolic resin composites. High Performance Polymers, 28(5), 505–517. https://doi.org/10.1177/0954008315587953
21. Zhang, L., Ni, C., Zhu, C., Jiang, X., Liu, Y., & Huang, B. (2009). Preparation and adsorption properties of chelating resins from thiosemicarbazide and formaldehyde. Journal of Applied Polymer Science, 112(4), 2455–2461. https://doi.org/10.1002/app.29627
22. Gao, J., Liu, Y., & Yang, L. (1999). Thermal stability of boron-containing phenol formaldehyde resin. Polymer Degradation and Stability, 63(1), 19–22. https://doi.org/10.1016/s0141-3910(98)00056-1
23. Alasadi, Alhawraa & Al-Sawaad, Hadi & Alwaaly, Ahmed. (2023). Synthesis, Characterization and evaluation of two organic compounds as corrosion inhibitors for carbon steel alloy (C1010) in acidic medium of 0.1M HCl. Journal of Kufa for Chemical Sciences. 2. 143-162. http://dx.doi.org/10.36329/jkcm/2022/v2.i9.13292
24. Zhang, F., Deng, S., Wei, G., & Li, X. (2023). Alternanthera philoxeroides extract as a corrosion inhibitor for steel in CL3CCOOH solution. International Journal of Electrochemical Science, 18(3), 100057. https://doi.org/10.1016/j.ijoes.2023.100057
25. Mustafa, F. A., Al-Sawaad, H. Z., & Saki, T. A. (2024). Evaluation of boron-modified guanidine resin as corrosion inhibitors for carbon steel alloy against acidic medium of

hydrochloric acid. Mor. J. Chem., 12(2), 614-626. https://doi.org/10.48317/IMIST.PRSM/morjchem-v12i2.45805
26. Wang, L., Zheng, H., Zi, X.-M., Zhang, S.-W., Peng, L., & Xiong, J. (2016). Evaluation of inhibition efficiency of 1-(2-pyridylazo) -2-naphthol and bromide ion on the corrosion of mild steel in sulphuric acid solution. International Journal of Electrochemical Science, 11(8), 6609–6626. https://doi.org/10.20964/2016.08.17
27. Pushpanjali, Rao, S. A., & Rao, P. (2017). Corrosion inhibition and adsorption behavior of Murraya koenigii extract for corrosion control of aluminum in hydrochloric acid medium. Surface Engineering and Applied Electrochemistry, 53(5), 475–485. https://doi.org/10.3103/s1068375517050088
28. Sanumi O. J., Saliu O. D., & Makhatha M. E. (2021). Alternative surface localization studies and electrochemical investigation of tyrosine hybridized poly (ethylene glycol) for corrosion inhibition of mild steel. Journal of Materials Research and Technology, 13, 700–715. https://doi.org/10.1016/j.jmrt.2021.05.007
29. Shivakumar S. S., & Mohana K. N. (2013). Corrosion behavior and adsorption thermodynamics of some Schiff bases on mild steel corrosion in Industrial Water Medium. International Journal of Corrosion, 2013, 1–13. https://doi.org/10.1155/2013/543204
30. Moustafa A. H., Abdel-Rahman H. H., Mabrouk D. F., & Omar A. Z. (2022). Mass transfer role in electropolishing of Carbone steel in H3PO4 containing amino acids: Electrochemical, computational, SEM/EDX, and Stylus Profilometer investigation. Alexandria Engineering Journal, 61(8), 6305–6327. https://doi.org/10.1016/j.aej.2021.11.062
31. Chaouiki A., Chafiq M., Lgaz H., Al-Hadeethi M. R., Ali I. H., Masroor S., & Chung I.-M. (2020). Green corrosion inhibition of mild steel by hydrazone derivatives in 1.0 M HCl. Coatings, 10(7), 640. https://doi.org/10.3390/coatings10070640
32. Okewale A. O., & Adesina O. A. (2020). Kinetics and thermodynamic study of corrosion inhibition of mild steel in 1.5m hcl medium using cocoa leaf extract as inhibitor. Journal of Applied Sciences and Environmental Management, 24(1), 37. https://doi.org/10.4314/jasem.v24i1.6
33. Manssouri M., Znini M., Lakbaibi Z., Ansari A., & El Ouadi Y. (2020). Experimental and computational studies of perillaldehyde isolated from Ammodaucus leucotrichus essential oil as a green corrosion inhibitor for mild steel in 1.0 M HCL. Chemical Papers, 75(3), 1103–1114. https://doi.org/10.1007/s11696-020-01353-5
34. Dalhatu S. N., Modu K. A., Mahmoud A. A., Zango Z. U., Umar A. B., Usman F., Dennis J. O., Alsadig A., Ibnaouf K. H., & Aldaghri O. A. (2023). L-arginine grafted chitosan as corrosion inhibitor for mild steel protection. Polymers, 15(2), 398. https://doi.org/10.3390/polym15020398
35. Zhang Y., Zhang S., Tan B., Guo L., & Li H. (2021). Solvothermal synthesis of functionalized carbon dots from amino acid as an eco-friendly corrosion inhibitor for copper in sulfuric acid solution. Journal of Colloid and Interface Science, 604, 1–14. https://doi.org/10.1016/j.jcis.2021.07.034
36. Yun J., Chen L., Zhao H., Zhang X., Ye W., & Zhu D. (2018). Boric acid as a coupling agent for preparation of phenolic resin containing boron and silicon with enhanced char yield. Macromolecular Rapid Communications, 40(17). https://doi.org/10.1002/marc.201800702

IRAQI Academic Scientific Journals
Samarra Journal of Pure and Applied Science
SJPAS
مجلة سامراء للعلوم الصرفة والتطبيقية
www.sjpas.com
p ISSN: 2663-7405
e ISSN: 2789-6838

تقييم راتنجات السيمكارباز ايد والثايوسيميكاربازيد المعدلة بالبورون كمثبطات لتآكل سبائك الصلب الكاربوني في البيئة الحامضية

مصطفى فتحي علي*، تحسن علي صاكي، هادي زيارة محمد
قسم الكيمياء، كلية العلوم، جامعة البصرة، العراق

معلومات البحث:
تأريخ الاستلام: 2024/03/23
تأريخ التعديل: 2024/04/20
تأريخ القبـــول: 2024/06/10
تأريخ الـنشر: 2025/03/30
الكلمات المفتاحية:
سيميكارباز ايد-فورمالديهايد، ثايوسيميكارباز ايد-فورمالديهايد، حامض البوريك، مثبطات التآكل، الراتنجات

معلومات المؤلف

الايميل:
Tahseen.saki@uobasrah.edu.iq
الموبايل: +964 781 192 3127

الخلاصة:

إنّ القلق بشأن تأثير التآكل على السلامة الهيكلية للأسطح المعدنية طويل الأمد. لذا تُستخدم مثبطات التآكل بشكل روتيني في الأنشطة الصناعية. اعتمد هذا البحث على تحضير نوعين من المثبطات: راتنجات السيميكاربازيد-فورمالدهايد المعدلة بالبورون (SFB) المشتقة من السيميكاربازيد، والفورمالدهيد، وحامض البوريك، والمثبط الآخر راتنجات الثايوسيميكاربازيد-فورمالدهايد المعدلة بالبورون (TSFB) المشتق من الثايوسيميكاربازيد، والفورمالدهيد، وحامض البوريك، وتمت دراستها باستخدام تقنيات FTIR وTGA. تم تقييمها كمثبطات لتآكل سبائك الفولاذ الكاربوني في بيئة حامضية اكالة من حامض الهيدروكلوريك 0.1 مولاري عند درجات حرارة متعددة (25، 35، 45، 55) درجة مئوية وبتراكيز مختلفة لكلا المثبطين كلّ على حدة، حيث أعطى (SFB) أفضل كفاءة تثبيط عند تركيز 4 جزء بالمليون بينما أفضل كفاءة تثبيطية كانت للـ (TSFB) عندما كان تركيزه 10 جزء بالمليون.